

Equi-Axed Grain Formation in Electrodeposited Sn-Bi

E. SANDNES,¹ M.E. WILLIAMS,¹ M.D. VAUDIN,² and G.R. STAFFORD^{1,3}

1.—Metallurgy Division, MSEL, NIST, Gaithersburg, MD 20899-8551, USA. 2.—Ceramics Division, MSEL, NIST, Gaithersburg, MD 20899-8520, USA. 3.—e-mail: gery.stafford@nist.gov

Sn is widely used as a coating in the electronics industry because it provides excellent solderability, ductility, electrical conductivity, and corrosion resistance. However, Sn whiskers have been observed to grow spontaneously from Sn electrodeposits and are known to cause short circuits in fine-pitched pre-tinned electrical components. We report here a deposition strategy that produces an equi-axed and size-tunable grain structure in Sn-Bi alloys electrodeposited from a commercial bright Sn electrolyte. An equi-axed grain structure should allow a more uniform creep to relieve compressive stress with no localized surface disturbance. The standard potential for Bi is about 0.45 V more positive than Sn. Pulsed deposition can selectively turn on and off the Sn deposition reaction. During the off cycle, a displacement reaction between metallic Sn on the electrode surface and Bi^{3+} in solution selectively dissolves Sn and deposits Bi, effectively terminating the growth from the previous cycle and forcing the Sn to nucleate a new grain on the Bi-enriched surface. The grain size is tunable by varying the pulsing conditions, and an equi-axed structure can be obtained with as little as 3 at.% Bi. This surface enrichment of Bi by potential modulation is similar to that which occurs naturally in Sn-Pb, and provides an avenue for breaking up the columnar grain structure inherent to pure Sn, thus providing an additional diffusion path for Sn that may prevent whisker growth.

Key words: Sn whiskers, electrodeposition, creep, solder, Pb-free

INTRODUCTION

Sn is widely used as a coating in the electronics industry because it provides excellent solderability, ductility, electrical conductivity, and corrosion resistance. However, Sn whiskers have been observed to grow spontaneously from Sn electrodeposits and are known to cause short circuits in fine-pitched pre-tinned electrical components. In the 1960s, the addition of a few percent of Pb to Sn was found to greatly reduce the tendency to form whiskers.¹ However, recent demand for Pb-free surface finishes for ecological manufacturing of electronic components has renewed interest in understanding whisker growth and developing whisker mitigation strategies. It is widely recognized that compressive stress is a necessary, but insufficient, condition for whisker growth.^{2,3} In addition to compressive stress,

commonly observed energy relaxation mechanisms such as grain growth and recrystallization must be impeded, i.e., grain-boundary pinning.^{3,4} As a consequence, the deposit microstructure may be as important as the residual stress state in determining whisker propensity.

In a previous paper⁵ we examined the residual stresses and microstructure of pure Sn, Sn-Cu, and Sn-Pb alloys electrodeposited onto phosphor bronze cantilever beam electrodes. Compressive stresses on the order of -15 MPa were measured in high-purity (metals basis) bright Sn electrodeposits within 15 min after plating. This is very close to the yield stress for electrodeposited Sn. We further observed that the codeposition of a few atomic percent Cu significantly increased the compressive stress in the Sn to -36 MPa while the codeposition of Pb reduced the compressive stress to -4 MPa. We believe that the increase/decrease in compressive stress for the alloys with respect to pure Sn is due to volume changes caused by the precipitation of $\text{Cu}_6\text{Sn}_5/\text{Pb}$

(Received September 26, 2007; accepted December 5, 2007;
published online December 29, 2007)

particles by metallurgical precipitation from the supersaturated Sn-Cu/Sn-Pb solid solution formed during plating.

The deposit microstructure contributes to the film's response to any residual stress. For example, if the compressive stress in the deposit relaxes by Coble creep (grain boundary transport of Sn and vacancies), then for pure Sn and Sn-Cu, both of which have columnar structures, the creep response is a flow of Sn toward the free surface.⁵ In the case of pure Sn, hillocks are formed due to extensive lateral grain boundary migration. In the case of Sn-Cu, precipitated Cu_6Sn_5 effectively pins the Sn grain boundaries. The lack of lateral grain boundary mobility of the columnar structure in the Sn-Cu deposits promotes whisker formation by maintaining a laterally small grain where Sn flux accumulates. In contrast to Sn and Sn-Cu, the addition of Pb causes an equi-axed grain structure to develop.^{5,6} As a consequence, transport between interior grain faces permits uniform swelling of the deposit thickness and no localized surface disturbance.

Based on these observations, a possible whisker mitigation strategy is to employ plating conditions and/or additives to the electrolyte that break up the columnar structure and promote the formation of grain boundaries parallel to the deposit surface as in the case of Sn-Pb. Such boundaries would allow a more uniform creep of electrodeposits to relieve compressive stress. The most straightforward approach is the use of pulsed deposition. The use of high deposition overpotentials and periodically setting the deposition current to zero to allow diffusion gradients of Sn^{2+} and essential plating additives to relax can promote the nucleation of new grains on the subsequent pulse. An alternative approach is the use of plating additives or alloying elements that promote the nucleation of new Sn grains. Since Pb seems to do this rather well, it might first be helpful to identify some of the attributes of the Sn-Pb system that might be worth emulating.

The standard reduction potentials of Sn and Pb are within 10 mV of each other, Pb being the more noble. As a consequence, a full range of Sn-Pb alloys is possible without the use of complexing agents. The reduction process is 100% efficient due to the poor kinetics (high overpotential) for hydrogen evolution on both metals. Several observations have been reported in the literature when Pb^{2+} is added to an additive-free Sn plating bath. The electrochemical kinetics that govern the deposition of each metal does not change when the alloy is deposited; the voltammetric curves are simply additive in both the kinetic-controlled and mass-transfer-controlled regimes.⁷⁻⁹ This tends to favor Pb deposition due to its higher exchange current and diffusion coefficient. Various organic additives are typically used to help eliminate dendritic growth and to promote a uniform current distribution. This is achieved by impeding the deposition kinetics for both species. The higher overpotential results in significant grain

refinement. However, in contrast to the additive-free plating baths, the presence of Pb^{2+} causes a significant inhibition in the Sn deposition kinetics.^{8,10} The overpotential for Sn deposition increases as Pb^{2+} is added to the plating bath, a clear electrochemical signature that Pb poisons Sn deposition.

The morphology of Sn and Sn-Pb has been examined on both glassy carbon and polycrystalline Au substrates from HBF_4 -based electrolyte.^{11,12} The deposition of pure Sn results in well-defined crystals with a tetragonal shape. In the presence of Pb, the microstructure of the Sn changes dramatically and resembles the microstructure of pure Pb, i.e., rounded nuclei that are similar in size. Microscopic examination indicates that the Pb forms small islands on the Sn, which tends to inhibit Sn on Sn deposition. This has been explained in terms of the underpotential deposition (UPD) of Pb onto Sn.¹¹ These authors further found that the codeposition of Pb significantly reduces any crystallographic texture in the Sn and prevents the formation of dendrites. More recently it has been shown that Pb codeposition alters the grain structure of Sn from columnar to equi-axed,^{5,6} presumably through this mechanism of inhibiting Sn on Sn deposition. It should be noted in any discussion of deposit morphology or phase distribution that as-deposited Sn-Pb alloys are metastable and that microstructural evolution in the form of phase separation and coarsening has been observed within days of deposition.¹³

A shortlist of potential alloying elements can be gathered from candidate Pb-free solders, namely bismuth, indium, silver, zinc, and antimony.¹⁴ Sn-Zn and Sn-Bi are similar to Sn-Pb in that the equilibrium phase diagrams indicate that no alloying occurs, other than the terminal solid solutions.¹⁵ Whereas the standard potential for Zn is about -0.62 V with respect to that of Sn, Bi is about 0.45 V more noble than Sn. This makes Sn-Bi rather attractive in that the potentials are close enough together for codeposition of a variety of alloy compositions under steady-state conditions, yet far enough apart that pulsed deposition can selectively turn on and off the Sn deposition reaction. This can lead to surface enrichment of Bi by potential modulation, similar to the Pb deposition on Sn that occurs naturally. More importantly, this may provide an avenue for breaking up the columnar grain structure inherent to pure Sn.

The electrodeposition of Sn-Bi alloys from methane sulfonic acid (MSA)-based electrolyte has been reported.^{14,16} The 0.45 V difference in deposition potentials gives rise to alloy compositions ranging from 10 at.% to 100 at.% Bi that can be accessed by varying the current density. Alloys containing less than 10 at.% Bi were reported to have a morphology similar to that of matte Sn.¹⁴ Fracture surfaces clearly showed that the Bi particles were segregated along the grain boundaries. These micrographs also indicated that the Sn grains were columnar,

suggesting that Bi is not as surface active as Pb and that pulsed deposition might be required to break up the columnar grain structure. In this paper, we examine the electrodeposition of pure Sn and Sn-Bi alloys using both direct current (DC) and pulsed current (PC) deposition in an effort to promote an equi-axed grain structure in the Sn. The influence of deposition conditions and electrolyte composition on the crystallographic texture of the Sn is also reported.

EXPERIMENTAL METHODS

Pure Sn was electrodeposited from a commercial MSA-based bright Sn plating solution using distilled water that was further purified to 18.3 M Ω cm using an EASY pure ultraviolet (UV) ultrapure water system (Barnstead*). The concentration of Sn²⁺ in the electrolyte was 0.379 mol L⁻¹. Pure Sn films were electrodeposited onto flat, 152- μ m-thick phosphor bronze substrates (nominal atomic fraction Cu-2.7% Sn-0.7% P) that had been wet-polished to 0.3 μ m alumina. The substrate was attached to a rotating disk electrode assembly and rotated during plating at 100 rotations per minute in order to establish reproducible hydrodynamic conditions. This rotation speed creates a uniform hydrodynamic boundary layer approximately 40 μ m thick along the electrode surface.¹⁷ The exposed electrode area was 3.0 cm². Plating was performed under a variety of galvanostatic pulsing conditions in 1 L of solution at 25 \pm 0.5°C. The deposition was controlled by a potentiostat/galvanostat (model 173) together with a universal programmer (model 175), both from Princeton Applied Research, EG&G Company. The average deposit thickness was 16 μ m (determined by charge assuming 100% current efficiency). The anode was a 99.999% pure Sn sheet and was placed underneath and parallel to the rotating working electrode. No reference electrode was used in the pure Sn deposition experiments.

Sn-Bi alloys were electrodeposited by the addition of Bi(NO₃)₃ · H₂O (Sigma-Aldrich, Inc., USA) to the commercial bright Sn plating solution at concentrations of 0.010 mol L⁻¹ and 0.040 mol L⁻¹. Alloys were electrodeposited onto stationary 0.5-mm-thick planar copper sheet (99.998%, Johnson Matthey) that was covered with micromask stop-off lacquer at the back and sides, exposing an area of 1.5 cm². The exposed Cu surface was wet-polished using SiC-paper #2400 and #4000 (Struers, Inc.) followed by a 1 μ m alumina slurry. All electrodes were rinsed thoroughly with ethanol and distilled water and directly immersed into the electrolyte. The rotating disk assembly used in the pure Sn deposits described above was not used for depositing

the Sn-Bi alloys in order to ensure a low deposition rate for Bi which is diffusion limited. The Sn-Bi alloys were electrodeposited in a single-compartment glass cell covered with a plastic film to prevent air from entering the compartment. An Ar purge of the head-space above the electrolyte was maintained at all times. A platinum counterelectrode was positioned in the same compartment as the working electrode. A saturated Hg sulfate electrode (SSE) was used as a reference electrode, and a Vycor-tipped bridge filled with 0.1 mol L⁻¹ H₂SO₄ separated the SSE from the working compartment. The Sn-Bi alloys were electrodeposited galvanostatically using a variety of pulsing conditions.

Linear sweep voltammetry was performed in the bright Sn plating solution containing 0.010 mol L⁻¹ Bi³⁺. The working electrode was a cross-sectioned 0.8-mm-diameter tungsten wire sealed in glass. The electrode was wet-polished with SiC-paper #2400 and #4000 and rinsed thoroughly with acetone, ethanol, and distilled water prior to use. A platinum counterelectrode and SSE reference electrode were positioned in the same compartment as the working electrode. The deposition of Sn-Bi alloys and voltammetry were performed using an Autolab PGSTAT 302 potentiostat/galvanostat from Eco Chemie B.V.

The electrodeposits were examined by X-ray diffraction (XRD), using a Siemens D-500 diffractometer with Cu-K α radiation, and by field-emission scanning electron microscope (SEM) using a Hitachi S4700 operating at 5 kV and 30 μ A, at a working distance of 22 mm. Cross-sections were prepared using a dual-beam focused ion beam (FIB) model DB620 (FEI Company). The milling was done at a 52 degree tilt with a 30 kV Ga ion beam operating at 11,500 pA for the initial trench milling, 2700 pA down to 150 pA for cutting the cross-sectioned wall, and a reduced current of 11 pA for fine cleaning of the milled wall surface in an effort to minimize the Sn-Ga reaction on the cross sectioned surface. FIB images were taken with the Ga ion beam, also at a current of 11 pA. Alloy composition was determined with a JEOL model 840A scanning electron microscope (SEM) using energy-dispersive spectroscopy (EDS), Noran System 5500, with elemental standards for Sn and Bi. All measurements were performed with an accelerating voltage of 15 kV, a probe current of 1150 pA, and a 100 s acquisition time. The reported compositions are an average of 15 independent measurements on the as-deposited surface.

RESULTS

Pure Sn Deposition

Several plating conditions were examined with the intent of breaking up the columnar grain structure inherent to bright Sn. Table I shows four conditions that are representative of deposition

*Certain trade names are mentioned for experimental information only; in no case does it imply a recommendation or endorsement by NIST.

Table I. Deposition Conditions, Bi³⁺ Concentration, Alloy Composition, and Summary of Crystallographic Texture of Selected Sn and Sn-Bi Electrodeposits

Deposit Figure	Bi ³⁺ Concentration mol L ⁻¹	Pulse #1 Current mA cm ⁻²	Pulse #1 Time s	Pulse #2 Current mA cm ⁻²	Pulse #2 Time s	Preferred Orientation <i>hkl</i>	Highest <i>p(hkl)</i>	Lowest <i>p(hkl)</i>	Bi Fraction in Alloy at. %
<i>Pure Sn</i>									
1a	0	60	DC	N/A	N/A	011	3.35	0.01	0
1b	0	60	20	0	2	332	3.16	0.05	0
1c	0	60	0.5	0	0.05	220	4.92	0.005	0
1d	0	60	10	300	1	013	2.25	0.05	0
<i>Sn-Bi</i>									
5a	0.04	40	DC	N/A	N/A	011	2.06	0.15	9.6 ± 1.1
5b	0.01	40	30	0	136	011	1.27	0.59	2.8 ± 0.8
5c	0.04	40	30	0	5	040	2.31	0.12	11.4 ± 1.0
5d	0.04	40	30	0	136	013	2.94	0.59	15.0 ± 1.0

using DC, long on/off times, short on/off times, and pulsing to high current density. The crystallographic texture of the electrodeposits is also summarized in Table I while the FIB cross-sections are shown in Fig. 1. These images were taken approximately 10 days after deposition. Figure 1a is a typical cross-section of a deposit formed galvanostatically using a current density of 60 mA cm⁻² DC. The grains are columnar, extending from the substrate to the surface with little variation in width. The average lateral grain size is on the order of 1.0 μm. Our first attempt to break up the columnar structure simply involved pulsing the deposition current. During the off-time (zero current) the diffusion gradients of Sn²⁺ and essential plating additives relax. The surface concentration of Sn²⁺ approaches the bulk value while the plating additives approach their equilibrium surface concentration. We calculate that this takes about 1.3 s, based on the 40 μm diffusion layer thickness and an estimated diffusion coefficient of 4 × 10⁻⁶ cm² s⁻¹. It was expected that this would promote the nucleation of new grains on the subsequent pulse. Figure 1b shows the cross-section of a deposit pulsed between 60 mA cm⁻² for 20 s and 0 mA cm⁻² for 2 s. Under this deposition condition, a pulse occurs about every 1 μm of deposit thickness. The FIB image shows that the pulsed deposit retains the columnar structure of the DC deposit. The absence of lateral grain boundaries indicates that existing grains grow in preference to the nucleation of new grains of different crystallographic orientation. Off times of up to 10 s were examined with little change in the columnar grain structure. Reducing the pulse width down to 500 ms while maintaining the 90% duty cycle (Fig. 1c) also did little to change the grain structure or size. The last deposition condition reported here for pure Sn consists of a 10 s growth pulse at 60 mA cm⁻² and a 1 s nucleation pulse at 300 mA cm⁻². There is no off time; rather the electrode is pulsed into H₂ evolution in an effort to disrupt Sn growth and promote nucleation of new grains. Pulsing into H₂ evolution can be beneficial in two ways. The higher deposition overpotential associated with the pulse can directly lead to the nucleation of new grains. Secondly, H₂ evolution can create a localized pH increase and lead to Sn(OH)₂ precipitation at the electrode surface, which would be expected to impede the growth of existing grains. However, one can see from Fig. 1d that the columnar grain structure remains intact. It does appear nonetheless that some lateral grain refinement was achieved by this pulsing scheme. It is also apparent that this deposit is noticeably thinner since pulsing into H₂ evolution reduces the current efficiency for Sn deposition.

Figure 2 shows the X-ray diffraction patterns for the deposits shown in Fig. 1. Although the various pulsing schemes failed to alter the columnar structure of the Sn, the relative intensities of the diffraction peaks vary considerably among the four

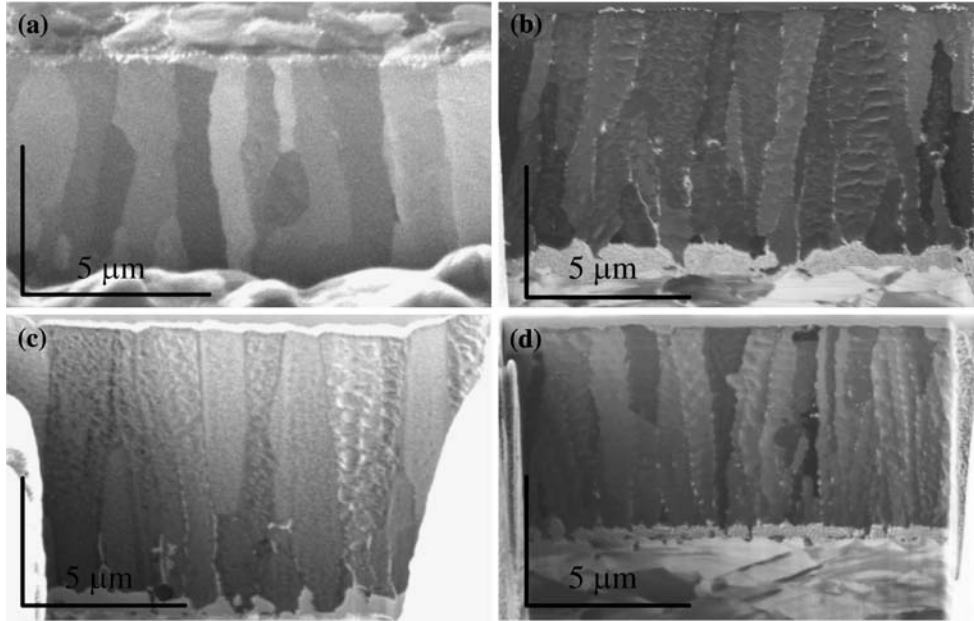


Fig. 1. SEM images of FIB'ed 16- μm -thick (nominal) bright Sn, electrodeposited from 0.379 mol L⁻¹ Sn MSA electrolyte at: (a) 60 mA cm⁻² (DC), (b) pulsed 60 mA cm⁻² for 20 s followed by open circuit for 2 s, (c) pulsed 60 mA cm⁻² for 500 ms followed by open circuit for 50 ms, (d) pulsed 60 mA cm⁻² for 10 s followed by 300 mA cm⁻² for 1 s.

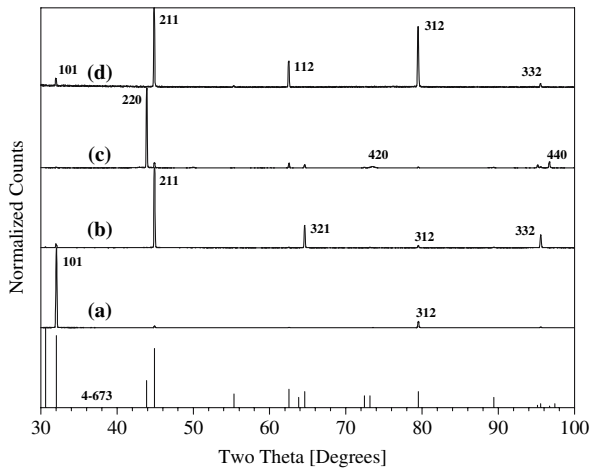


Fig. 2. X-ray diffraction patterns (Cu-K α_1) for the electrodeposits shown in Fig. 1.

samples, suggesting variation of the crystallographic texture. A treatment by Mueller¹⁸ appropriate for fiber texture was applied to the X-ray intensity data, in which the integrated intensity of each peak, $I(hkl)$, was divided by the Joint Committee on Powder Diffraction Standards (JCPDS) intensity for that peak, $I_o(hkl)$. The JCPDS pattern is typically collected from a randomly oriented sample. The ratio for each Bragg peak was scaled by dividing it by the average of all the ratios for the observed peaks to give a preferred orientation factor, $p(hkl)$, for each hkl plane. This is shown mathematically in Eq. 1 where n is the total number of reflections in the X-ray pattern.

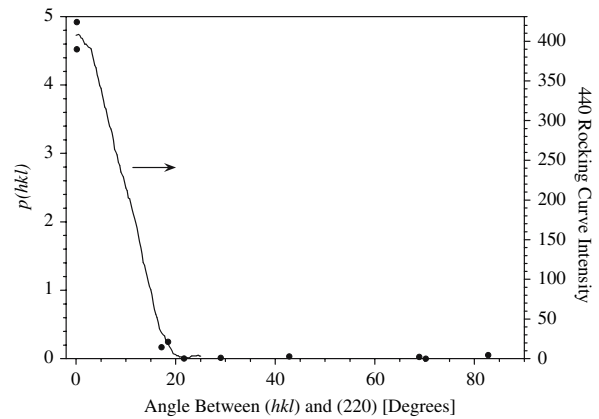


Fig. 3. Plot of $p(hkl)$ for deposit 1c (pulsed 60 mA cm⁻² for 500 ms followed by open circuit for 50 ms) as a function of angle with respect to the (220) planes (●). The 440 rocking curve is also shown (—) arbitrarily scaled to the average of the $p(220)$ and $p(440)$.

$$p(hkl) = \frac{I(hkl)/I_o(hkl)}{\frac{1}{n} \sum [I(hkl)/I_o(hkl)]} \quad (1)$$

A randomly oriented film will have $p(hkl)$ values equal to 1.0 for all (hkl) planes. A large deviation from unity suggests that the deposit is textured with the diffracting planes producing the largest $p(hkl)$ preferentially parallel to the film plane. Tin presents particular problems for texture analysis since one of the possible texture directions, normal to (001), is difficult to probe because the only 00 l peak that is allowed and obtainable using a Cu-K α_1 source is 004, which is a very weak peak with a 2θ

value of 151.1 degrees and is not listed in any of the JCPDS entries for Sn. The $p(hkl)$ data are summarized in Table I by the maximum value, the indices hkl of the peak giving the maximum, and the minimum $p(hkl)$ value. It is clear that considerable texture has been generated by the various deposition processes; however, the textured planes are radically different for each sample. The $p(hkl)$ values were plotted versus the respective angle between the textured and diffracting planes. An example is shown in Fig. 3 for the film shown in Fig. 1c. The sample shows (110) texture with a maximum $p(220)$ of about 5, which decreases to zero as the angle increases from zero. In addition to $p(hkl)$ we plot in Fig. 3 the 440 rocking curve, with intensity arbitrarily scaled to the average of the $p(220)$ and $p(440)$; the agreement is excellent. The quantitative measure of texture is multiples of a random distribution (MRD). This is the volume fraction of a sample at a particular orientation divided by the volume fraction of a randomly oriented sample at the same orientation.¹⁹ It should be emphasized that there is no implied equivalence between the $p(hkl)$ and MRD.

Sn-Bi Alloy Deposition

Another approach to breaking up the grain structure is by codepositing another metal that inhibits Sn deposition. This can occur naturally, as in the case of Sn-Pb, or artificially using pulsed deposition to selectively turn on and off the Sn

deposition reaction. Figure 4 shows a cyclic voltammogram for a W electrode in the bright Sn electrolyte containing $0.010 \text{ mol L}^{-1} \text{ Bi}^{3+}$. The inset shows the voltammetry for Bi^{3+} alone. Bismuth deposition initiates at about -0.56 V with respect to the SSE reference electrode. The current peak and subsequent current decay are consistent with diffusion-limited deposition of Bi. We have estimated the steady-state diffusion-limited current to be about 0.5 mA cm^{-2} , based on a Bi^{3+} diffusion coefficient of $1.72 \times 10^{-6} \text{ cm}^2 \text{ s}^{-1}$.²⁰ Upon reversing the potential, the Bi can be completely stripped from the tungsten at potentials more positive than -0.5 V . If the potential is swept to more negative values, Sn codeposition is observed at about -0.95 V , about 0.4 V more negative than that for Bi deposition. In this potential region, Sn-Bi alloys having a wide range of composition can be electrodeposited. For example, since Bi deposition is limited by diffusion (about 0.5 mA cm^{-2}), a film deposited galvanostatically at 40 mA cm^{-2} will have a Bi content of about 1.0 at.%. Smaller currents will lead to a higher Bi content since only the rate for Sn deposition is reduced. If, on the other hand, the current is periodically pulsed to a value of zero, then during the off time the electrode will sit at the rest potential for Sn, or about -0.9 V . At this potential a displacement reaction between metallic Sn on the electrode surface and Bi^{3+} in solution will occur, selectively dissolving Sn and depositing Bi, at a rate that is still limited by Bi^{3+} diffusion. The relevant reactions are shown in Fig. 4.

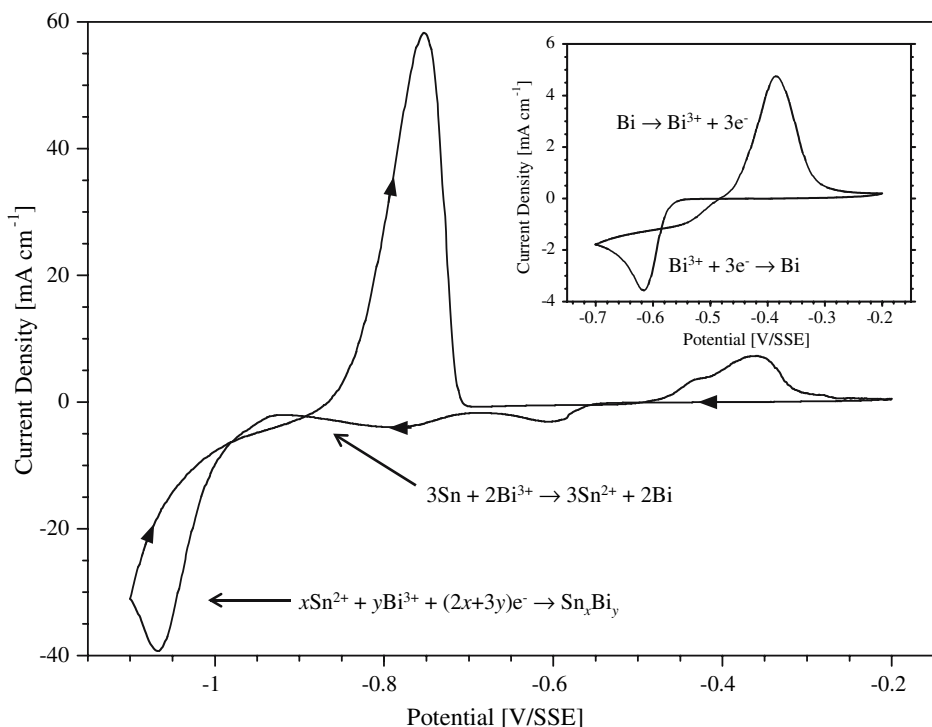


Fig. 4. Cyclic voltammogram on a W wire cross-section electrode in 0.379 mol L^{-1} Sn MSA containing $0.010 \text{ mol L}^{-1} \text{ Bi}^{3+}$ at a sweep rate of 50 mV s^{-1} . The inset shows voltammogram for Bi deposition/stripping in the same electrolyte.

Figure 5 shows FIB cross-sections of Sn-Bi alloys electrodeposited under a variety of deposition conditions, shown in Table I. Figure 5a is a typical cross-section of a deposit formed galvanostatically using a current density of 40 mA cm^{-2} DC, from an electrolyte containing $0.040 \text{ mol L}^{-1} \text{ Bi}^{3+}$. The deposit contains about 9.6 at.% Bi yet there is little indication, other than a slightly larger grain size and occasional transverse grain boundary, that the columnar structure inherent to bright Sn deposition has been significantly altered. One can conclude from this that Bi does not behave like Pb in terms of inhibiting the Sn deposition reaction and promoting an equi-axed grain structure. However if pulsed deposition is used, the displacement reaction that occurs during the off-cycle effectively terminates the growth from the previous cycle and forces the Sn to nucleate a new grain on the Bi-enriched surface. Figure 5b shows an example of pulsed deposition in electrolyte containing $0.010 \text{ mol L}^{-1} \text{ Bi}^{3+}$. The relatively low Bi^{3+} concentration required a significant off-time (136 s) to break up the columnar grain structure effectively. The average Bi composition of this deposit is 2.8 at.%, most of which is likely present at the grain boundaries. The cross-section in Fig. 5b shows the formation of nice equi-axed grains, similar to those observed for Sn-Pb.^{5,6} The average grain size appears to be about $3 \mu\text{m}$, whereas a pulse was introduced every $1 \mu\text{m}$ of deposit. It is fairly clear that some of the Sn grains continue to grow in spite of the Bi deposited during the off cycle, suggesting that the Bi layer is not continuous. However, the grain size can be further

reduced by increasing the concentration of Bi^{3+} in the electrolyte. Figure 5c shows a deposit cross-section obtained from a 5 s off time in an electrolyte containing $0.040 \text{ mol L}^{-1} \text{ Bi}^{3+}$. The average grain size is less than $2 \mu\text{m}$; however the average Bi content of the alloy has increased to 11.4 at.%. Increasing the off time to 136 s results in equi-axed grains, the size of which are consistent with the growth pulse. This is a clear indication that new Sn grains are nucleated with each pulse. This longer off time increases the average Bi alloy composition to 15.0 at.%.

Figure 6 shows the X-ray diffraction patterns for the deposits shown in Fig. 5. Small peaks from Bi were detected in addition to the Sn peaks. The $p(hkl)$ values were calculated from the integrated areas of the Sn peaks and, as before, highest and lowest $p(hkl)$ values and the reflection with the highest $p(hkl)$ are given in Table 1. Clearly the texture level is reduced, as would be expected when the film microstructure changes from columnar to equi-axed. The much larger value of the lowest $p(hkl)$ compared to the pure Sn films is the significant finding in this regard. There was also somewhat more consistency in the preferred orientation of these Sn-Bi samples. As expected, the films with the longest off period had the least amount of texture, based on the ratio of the highest/lowest $p(hkl)$. However, there was no convincing evidence that changes in texture were driving microstructure development. Rather, the texture changes appeared to be of much less importance than the significant change to an equi-axed microstructure.

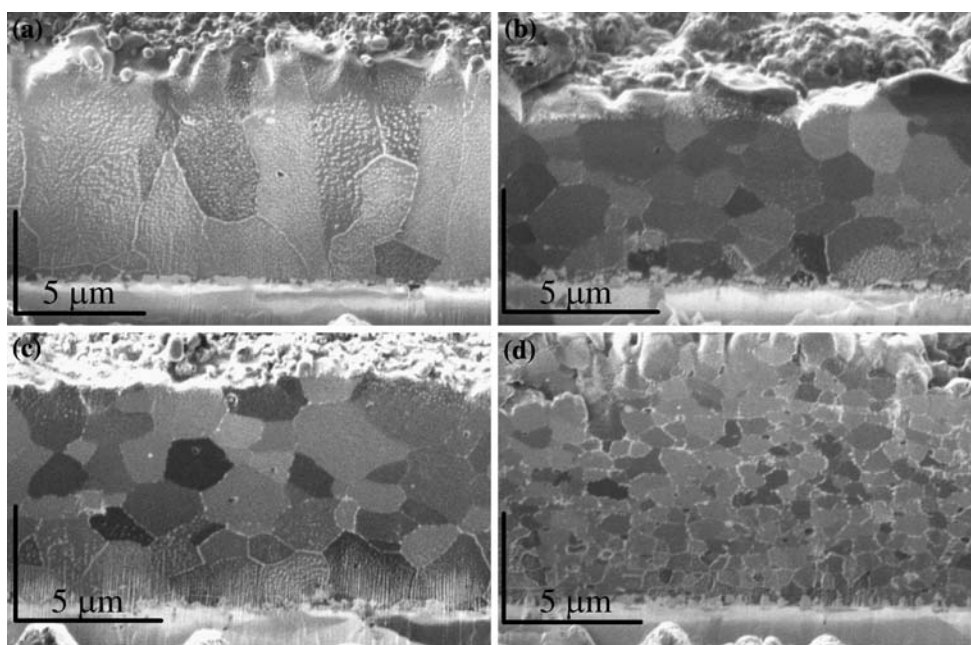


Fig. 5. SEM images of FIBed 15- μm -thick (nominal) bright Sn-Bi, electrodeposited from 0.379 mol L^{-1} Sn MSA electrolyte at (a) 40 mA cm^{-2} (DC), containing $40 \text{ mmol L}^{-1} \text{ Bi}^{3+}$, (b) pulsed 40 mA cm^{-2} for 30 s followed by open circuit for 136 s, containing $10 \text{ mmol L}^{-1} \text{ Bi}^{3+}$, (c) pulsed 40 mA cm^{-2} for 30 s followed by open circuit for 5 s, containing $40 \text{ mmol L}^{-1} \text{ Bi}^{3+}$, and (d) pulsed 40 mA cm^{-2} for 30 s followed by open circuit for 136 s, containing $40 \text{ mmol L}^{-1} \text{ Bi}^{3+}$.

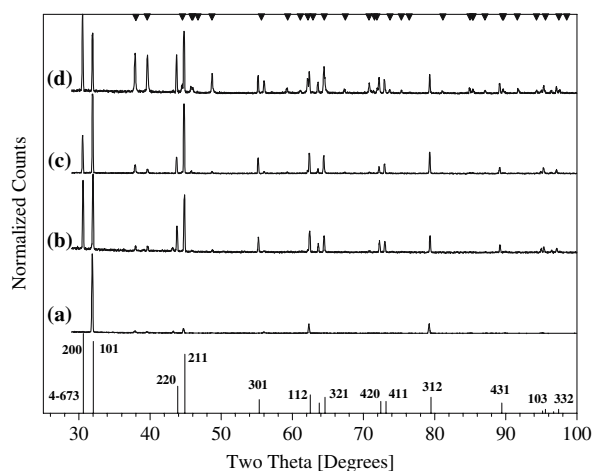


Fig. 6. X-ray diffraction patterns (Cu-K α_1) for electrodeposits shown in Fig. 5.

SUMMARY

We present a deposition strategy that produces an equi-axed and size-tunable grain structure in Sn-Bi alloys. Pulsed deposition is used to selectively turn on and off the Sn deposition reaction. Since the standard potential for Bi is about 0.45 V more positive than Sn in this electrolyte, during the off cycle a displacement reaction between metallic Sn on the electrode surface and Bi³⁺ in solution selectively dissolves Sn and deposits Bi, effectively terminating the growth from the previous cycle and forcing the Sn to nucleate a new grain on the Bi-enriched surface. The grain size is tunable by varying the pulsing conditions, and an equi-axed structure can be obtained with as little as 3 at.% Bi. This surface enrichment of Bi by potential modulation is similar to that which occurs naturally in Sn-Pb deposition, and provides an avenue for breaking up the columnar grain structure inherent to pure Sn, thus providing an additional diffusion path for Sn that may prevent whisker growth.

ACKNOWLEDGEMENTS

The authors gratefully acknowledge the technical contributions of Kil-Won Moon, William Boettinger, and David Kelley.

REFERENCES

1. S.M. Arnold, *Plating* 53, 96 (1966).
2. G.T. Galyon, *IEEE Trans. Electron. Packag. Manuf.* 28, 94 (2005).
3. J.W. Osenbach, J.M. DeLuca, B.D. Potteiger, A. Amin, and F.A. Baiocchi, *J. Mater. Sci.: Mater. Electron.* 18, 283 (2007).
4. R.M. Fisher, L.S. Darken, and K.G. Carroll, *Acta Metall.* 2, 368 (1954).
5. W.J. Boettinger, C.E. Johnson, L.A. Bendersky, K.-W. Moon, M.E. Williams, and G.R. Stafford, *Acta Mater.* 53, 5033 (2005).
6. W. Zhang and F. Schwager, *J. Electrochem. Soc.* 153, C337 (2006).
7. C.S. Chen, C.C. Wan, and Y.Y. Wang, *Trans. Inst. Met. Finish.* 76, 54 (1998).
8. J. Horkans, I.C.H. Chang, and P.C. Andricacos, *IBM J. Res. Dev.* 37, 97 (1993).
9. A.M. Pesco and H.Y. Cheh, *J. Electrochem. Soc.* 135, 1722 (1988).
10. J.-H. Kim, M.-S. Suh, and H.-S. Kwon, *Surf. Coat. Technol.* 56, 56 (1996).
11. I. Petersson and E. Ahlberg, *J. Electroanal. Chem.* 485, 166 (2000).
12. I. Petersson and E. Ahlberg, *J. Electroanal. Chem.* 485, 178 (2000).
13. F. Ogburn and H. Brown, *Plat. Surf. Finish.* 75, 58 (1988).
14. M. Jordon, *Trans. Inst. Met. Finish.* 75, 149 (1997).
15. *Binary Alloy Phase Diagrams*, T.B. Massalski, ed. (Metals Park, OH: American Society of Metals, 1986).
16. M.-S. Suh, C.-J. Park, and H.-S. Kwon, *Surf. Coat. Technol.* 200, 3527 (2006).
17. A.J. Bard and L.R. Faulkner, *Electrochemical Methods: Fundamentals and Applications* (New York, NY, 1980), p. 288.
18. M.H. Mueller, W.P. Chernock, and P.A. Beck, *Trans. AIME* 212, 39 (1958).
19. U.F. Kocks, C.N. Tome, and H.R. Wenk, eds., *Texture and Anisotropy: Preferred Orientations in Polycrystals and their Effect on Materials Properties* (Cambridge University Press, 1998).
20. E. Sandnes, M.E. Williams, U. Bertocci, M.D. Vaudin, and G.R. Stafford, *Electrochim. Acta* 52, 6221 (2007).